vaccines

MDPI

Article

N-terminal VP1 truncations favor *T*=1 norovirus-like particles

Ronja Pogan [1,2], Victor U. Weiss [3], Kevin Bond [4], Jasmin Dülfer [1], Christoph Krisp [5], Nicholas Lyktey [4], Jürgen Müller-Guhl [1,6], Samuele Zoratto [3], Günter Allmaier [3], Martin F. Jarrold [4], Cesar Muñoz-Fontela [6], Hartmut Schlüter [5], and Charlotte Uetrecht [1,2,*]

[1] Heinrich Pette Institute, Leibniz Institute for Experimental Virology, Hamburg, Germany
[2] European XFEL GmbH, Schenefeld, Germany
[3] Institute of Chemical Technologies and Analytics, TU Wien, Vienna, Austria
[4] Department of Chemistry, Indiana University, Bloomington, IN, USA
[5] Institute of Clinical Chemistry and Laboratory Medicine, Mass Spectrometric Proteomics Group, University Medical Center Hamburg - Eppendorf, Hamburg, Germany
[6] Bernhard Nocht Institute for Tropical Medicine and German Center for Infection Research (DZIF), Partner site Hamburg-Lübeck-Borstel-Riems, Hamburg, Germany.
* Correspondence: charlotte.uetrech@leibniz-hpi.com

Received: date; Accepted: date; Published: date

Abstract: Noroviruses cause immense sporadic gastroenteritis outbreaks worldwide. Emerging genotypes, which are divided based on VP1 sequence, further enhance this public threat. Self-assembling properties of the human norovirus major capsid protein VP1 are crucial for using virus-like particles (VLPs) for vaccine development. However, there is no vaccine available yet. Here, VLPs from different variants produced in insect cells are characterized in detail using a set of biophysical and structural tools. We are using native mass spectrometry, gas-phase electrophoretic mobility molecular analysis and proteomics to get clear insights into particle size, structure, composition as well as stability. Generally, noroviruses have been known to form mainly *T*=3 particles. Importantly, we identify a major truncation in the capsid proteins as a likely cause for the formation of merely *T*=1 particles. For vaccine development, particle production needs to be a reproducible, reliable process. Understanding the underlying processes in capsid size variation will help to produce particles of a defined capsid size presenting antigens consistent with intact virions. Next to vaccine production itself, this would be immensely beneficial for bio-/nano-technological approaches using viral particles as carriers or triggers for immunological reactions.

Keywords: norovirus, capsid assembly, native mass spectrometry, nES GEMMA, differential mobility analysis, CDMS

1. Introduction

A vast number of nonbacterial gastroenteritis cases worldwide is caused by human noroviruses (hNoVs) (1). Norovirus infection especially poses an acute threat to children, immunocompromised individuals and elderly people. Already a small number of particles is sufficient for infection (2). Gastroenteritis outbreaks happen worldwide with new hNoV-variants occurring sporadically.

Human noroviruses are non-enveloped and a member of the *Caliciviridae* family. They have a positive sense, single strand, approx. 7.7 kb RNA genome organized into three open reading frames (ORFs) and a poly(A) tail. ORF1 encodes non-structural proteins, ORF2 the major capsid protein VP1 and ORF 3 the minor structural protein VP2 (3, 4). Based on VP1, noroviruses can be classified into up to ten genogroups (GI-GX) and further into genotypes (5). Genogroups I, II, IV, VIII, and IX

infect humans. The prototypical GI.1 Norwalk was isolated from stool samples in Norwalk, Ohio in 1968 (6). Nowadays, mostly GII.4 and GII.17 strains have been identified as a cause of viral gastroenteritis outbreaks (7, 8).

There is no norovirus vaccine available, yet. The lack of a robust cell culture system and small animal models as well as the immense genetic diversity of hNoVs hinders its development to date. Although breakthroughs in developing a cell-culture system have been made in 2016 by Ettayebi et al (9), hNoV research has mostly been based on virus-like particles (VLPs). Current vaccine candidates are also using VLPs, mostly GI.1 and GII.4 VLPs. hNoVLPs can be produced by expressing VP1 in various systems, including insect cells, yeast, mammalian cells, and plants (10-13).

Generally, VP1 can be divided into two functionally and structurally distinct domains. The shell (S) domain, forming a scaffold around the genome, and a protruding (P) domain. In GI.1 Norwalk, the N-terminal 225 amino acids (aa) belong to the S-domain. The P-domain is further divided into subdomains P1 and an insertion P2 with P2 being most variable and involved in host-attachment and immunogenicity (14, 15). Self-assembling properties of VP1 allow next to fully formed, virion-resembling particles several other forms (16). These include P-dimer as well as 12-mer, 24-mer P-particles, where the P-domain only, with or without a tag respectively, is expressed in E.coli (17). Expression of the S-domain in the baculovirus-expression system results in thin-layered, small and smooth *T*=3 particles (18). In full-length VP1 particles, S and P domain are connected via a flexible hinge region (14). When expressed in eukaryotic systems, caliciviruses generally are known to assemble into VP1 180-mers with *T*=3 icosahedral symmetry. However, VP1 60-mers of *T*=1 symmetry have been described as byproducts of hNoVLP production coexisting with other particle sizes and independent of the expression system (19). Recently, also VP1 240-mers of *T*=4 symmetry have been described so far only for GII.4 variants expressed in insect cells as well as in plants (20, 21). In studies on virions of different norovirus variants *T*=3 as well as *T*=1 formations were detected (22).

Thus, hNoVLP particle sizes are polymorph and dynamic. Native mass spectrometry (MS) is a perfect biophysical tool to characterize these structural dynamics (23). Previously, VLPs of three different norovirus variants have been investigated with native MS (24, 25). In our previous work, we established the pH stability pattern of two norovirus variants, GI.1 West Chester and GII.17 Kawasaki (25). Stability was assessed in different ionic strength as well as pH and compared to results on Norwalk VLPs (24). In all three variants, *T*=3 particles were identified as the major population. Furthermore, GII.17 Kawasaki was resistant to changing conditions, while both GI variants disassembled upon alkaline treatment.

In order to characterize hNoVLPs in detail and gain more insights into size determination, we extended our previous native MS studies with a set of biophysical methods. Next to charge detection mass spectrometry (CDMS) for mass determination of heterogeneous particle populations and proteomics, we are using nano electrospray gas phase electrophoretic mobility molecular analysis (nES GEMMA) (26), especially suited to measure high-mass particles at low concentrations ((27, 28). Notably, this fast technique allows measurements at low ionic strength and with less concentrated sample.

We describe particle preparations from insect cells with sample batches, where *T*=1 only particles are detected. A major VP1 truncation was identified in all particle preparations forming these *T*=1 particles. We find that this size-limitation is genogroup and genotype-independent and cannot be rescued in different buffer conditions. This provides great implications for vaccine design and other applications of bio-nanoparticles, where size-homogeneity is highly favored.

2. Materials and Methods

VLP production and preparation

Full-length VP1 genes for GI.1 West Chester, GII.4 Saga 2006, GII.10 Vietnam, GII.17 Kawasaki308 and GII.17 Saitama T87 (GenBank accession numbers: AY502016.1, AB447457.1, AF504671.2

AF504671, LC037415.1, AII73747.1), were cloned and expressed in a baculovirus system (29, 30). After transfection of a bacmid containing the recombinant VP1 gene in Sf9 insect cells and incubation for 5–7 days, the culture medium was collected and centrifuged for 10 min at 3,000 rpm at 4°C. Subsequently, Hi5 insect cells were infected with recovered baculovirus and incubated for 5 days. After centrifuging the culture medium for 10 min at 3,000 rpm at 4°C and then 1 h at 6,500 rpm at 4°C, VLPs in the supernatant were concentrated by ultracentrifugation at 35,000 rpm (Beckman Ti45 rotor) for 2 h at 4°C. Furthermore, VLPs were further purified using CsCl equilibrium gradient ultracentrifugation at 35,000 rpm (Beckman SW56 rotor) for 18 h at 4°C. VLPs were pelleted for 2 h at 40,000 rpm (Beckman TLA55 rotor) at 4°C and solved in PBS (pH 7.4).

VP1 mapping

Trypsin digestion. For tryptic digestion followed by proteomic analysis, VLP samples in PBS at 15 μM VP1 were separated via sodium dodecyl sulfate polyacrylamide gel electrophoresis (SDS-PAGE) following the reported method (31). After staining with a solution containing 0.5% Coomassie brilliant blue R250, 50% ethanol and 7% acetic acid, respective gel bands were cut into small pieces and further processed according to Shevchenko et al. (32). After digestion, the samples were dried and thereafter dissolved in 0.1% formic acid (FA) and transferred into the autosampler. Tryptic peptides were separated on a nano-UPLC system (Dionex Ultimate 3000 UPLC system, Thermo Fisher Scientific) with a 50 cm C18 analytical column (Acclaim PepMap 100, 75 μm, 3 μm, Thermo Fisher Scientific) using a 60-min gradient with increasing acetonitrile concentration from 2 to 30%. Eluting peptides were desorbed and ionized with an electrospray-ionization (ESI) source into a tribrid mass spectrometer consisting of a quadrupole, linear ion-trap and an orbitrap (Fusion; Thermo Fisher Scientific) in data-dependent acquisition (DDA) mode. MS/MS-spectra were searched with the Sequest algorithm integrated in the Proteome Discoverer software version 2.0, against AY502016.1, AB447457.1, AF504671.2 AF504671, LC037415.1, AII73747, and a common contaminant protein database. Precursor ion and fragment ion mass tolerances were set to 10 ppm and 0.6 Da, respectively. Carbamidomethylation was set as a fixed modification oncysteine residues. Acetylation of the protein N terminus, N-terminal methionine loss, the oxidation of methionine, deamidation of asparagine and glutamine, and glutamine to pyroglutamate on the peptide N-Terminus were set as variable modifications. Only peptides with a high confidence (FDR of <1%) using a decoy database approach were accepted as identified.

Pepsin digestion. VLP samples were mixed 1:1 with denaturing buffer (300 mM phosphate buffer, pH 2.3, 6 M urea). Pepsin digestion of 100 pmol VP1 was performed online (Agilent Infinity 1260, Agilent Technologies) on a home packed pepsin column (IDEX guard column with an internal volume of 60 μL, Porozyme immobilized pepsin beads, Thermo Scientific) at a flow rate of 75 μL/min (0.4 % formic acid in water). Peptides were trapped in a trap column (OPTI-TRAP for peptides, Optimize Technologies) and separated on a reversed-phase analytical column (PLRP-S for Biomolecules, Agilent Technologies) using a 27 min gradient of 8-40 % organic solvent (0.4 % formic acid in acetonitrile) at 150 μL/min. MS was performed using an Orbitrap Fusion Tribrid in positive ESI data-dependent MS/MS acquisition mode (Orbitrap resolution 120000, 1 microscan, HCD 30 with dynamic exclusion). Precursor and fragment ions were searched and matched against a local protein database containing the proteins of interest in MaxQuant (version 1.5.7.0) using the Andromeda search engine. The digestion mode was set to "unspecific" and N-terminal acetylation, deamidation, oxidation and disulfide bond formation were included as variable modifications with a maximum number of 5 modifications per peptide. Peptides between 5 and 30 amino acids length were accepted. The MaxQuant default mass tolerances for precursor (4.5 ppm) and fragment (20 ppm) ions defined for the Thermo Orbitrap instrument were used for data search. The minimum score for successful identifications was set to 20 for unmodified and 40 for modified peptides.

Sample preparation

For mass spectrometry as well as nES GEMMA analysis, hNoVLP sample solutions were exchanged to 40 and 250 mM ammonium acetate solutions. Solution pH was adjusted between 5 and 9 using acetic acid and ammonia. For the solution exchange, Vivaspin 500 centrifugal concentrators (10,000 MWCO, Sartorius, Göttingen, Germany) or Zeba micro spin™ desalting colums 0.5 ml (7000 MWCO, Thermo Fisher Scientific, Rockford, IL, USA) were used. Generally, 5 filtration steps using spin filters and 3 steps using size-exclusion columns were employed. Samples were diluted to 10 μM VP1 protein or further diluted, if necessary, to obtain spectra.

Mass spectrometry

Conventional native MS measurements of VLPs were performed using a quadrupole time-of-flight (QToF) instrument Q-Tof 2 (Waters, Manchester, UK and MS Vision, Almere, the Netherlands) modified for high mass experiments (33). For electrospray ionization (ESI), capillaries were handmade by pulling borosilicate glass tubes (inner diameter 0.68 mm, outer diameter 1.2 mm with filament, World Precision Instruments, Sarasota, FL, USA) using a two-step program in a micropipette puller (Sutter Instruments, Novato, CA, USA) with a squared box filament (2.5x2.5 mm). Gold-coating of capillaries was performed using a sputter coater (Quorum Technologies., East Sussex, UK, 40 mA, 200 s, tooling factor of 2.3 and end bleed vacuum of 8×10^{-2} mbar argon or Safematic, Zizers, Switzerland, process pressure $5\text{x}10^{-2}$ mbar, process current 30.0 mA, coating time 100 s, 3 runs to vacuum limit $3\text{x}10^{-2}$ mbar Argon). Capillaries were opened on the sample cone of the mass spectrometer. Using a nanoESI source, ions were introduced into the vacuum at a source pressure of 10 mbar. Positive ion mode was used to record spectra. Generally, voltages of 1.45 kV and 165 V to the capillary and cone, respectively, were used and adjusted during spray-optimization. Xenon was used as a collision gas at a pressure of $1.7\text{x}10^{-2}$ mbar in order to enable better transmission of high-mass ions (34). MS profile and repetition frequency of the pusher pulse were adjusted to high mass range. For instrument calibration, a cesium iodide spectrum was recorded the same day. Analysis was performed using MassLynx V4.1 SCN 566 (Waters, Manchester, UK) and Massign (35).

Charge detection mass spectrometry (CDMS) was performed on a home-built CDMS instrument described in detail elsewhere (36) in order to enable measurements of heterogeneous complexes in the MDa range or larger. Briefly, charge and *m*/*z* of single ions are measured simultaneously using a charge conduction cylinder and electrostatic ion trap. In contrast to conventional QToF MS, CDMS sidesteps the need for charge states to be assigned. Ions were generated using an automated nano-ESI source (Nanomate, Advion, Ithaca, NY, USA) with a capillary voltage of approximately 1.7 kV. After entering a heated metal capillary, ions are transmitted using various ion optics to a dual hemispherical deflection energy analyzer, which selects ions with energies centered on 100 eV/z. Subsequently, ions enter a modified cone trap where they oscillate back and forth in a charge detection cylinder for 100 ms. Single ion masses were binned to generate mass spectra. Mass spectra were analyzed by fitting Gaussian peaks with Origin software (OriginPro 2016).

Gas-phase electrophoresis was performed on a nES GEMMA instrument (TSI Inc, Shoreview, MN, USA) consisting of a nES aerosol generator (model 3480) including a ^{210}Po α-particle source, an electrostatic classifier (model 3080) with a nano differential mobility analyzer (nDMA) and an n-butanol based ultrafine condensation particle counter (model 3025A). Briefly, particle-size determination is a function of the particles' trajectory in the nDMA chamber. The trajectory of a size-specific particle is based on the sheath flow of particle-free ambient air and an orthogonal electric field applied. Therefore, with a constant high laminar sheath flow of air and a variable electrical field, only specific particle sizes can successfully be transported to the particle counter device for detection. For electrospraying, polyimide coated fused silica capillaries (25 μm inner diameter, Polymicro, obtained via Optronis, Kehl, Germany) with in-house made tips (37) were used. Settings for a stable Taylor cone at the nES tip were chosen, typically around 2 kV resulting in approx. -375 nA current, 0.1 L/min CO_2 (Messer, Gumpoldskirchen, Austria) and 1.0 L/min filtered, dried ambient air. Four pounds per square inch differential (psid, approx. 27.6 kPa) were applied to additionally move the sample through the capillary. 15 L/min sheath flow filtered ambient air was

used to size-separate VLPs in an electrophoretic mobility diameter (EMD) range from 2 to 65 nm. The corresponding EMD size range was scanned for 120 s. Subsequently, the applied voltage was adjusted to starting values within a 30 s timeframe. Seven datasets (raw data obtained from instrument software, MacroIMS manager v2.0.1.0) were combined via their median to yield a corresponding spectrum. Lastly, Gauss peaks were fit to spectra via Origin software (OriginPro 2016) to obtain EMD values. EMD values were correlated to particle mass using MW-correlation either based on proteins (38) or VLPs (28).

3. Results

3.1 Truncated GII.4 Saga VP1 forms homogeneous T=1 particles

Here, we extend our previous investigations on GI.1 West Chester and GII.17 Kawasaki to other hNoVLP constructs. VLPs of an outbreak strain GII.4 Saga are produced in the same baculovirus-expression system. Native mass spectra reveal the lack of *T*=3 particles at neutral pH and moderate ionic strength (Figure 1). Notably, the identified peak distribution is almost baseline resolved indicating a highly homogeneous population annotated to VP1 60-mers or *T*=1 particles. An additional, unresolved peak distribution around 15,000 *m*/*z* relates to metastable ions. Metastable ions are commonly accompanying high-mass ions as these disintegrate partially in the ToF-analyzer, as such they cannot be targeted by selection in the quadrupole allowing differentiation from ions originating from the sample solution. Figure 1 also illustrates collision-induced dissociation (CID) products for GII.4 Saga. The *T*=1 ions (~ 150+ charges) dissociate via consecutive losses of VP1 monomers, with at least two subspecies in mass, as well as corresponding high mass ions, VP1 59-mer, 58-mer and 57-mer. Mass-assignment of the dissociated monomer suggests an N-terminal truncation of 45 amino acids (aa) of the main species and a subpopulation lacking 45 aa. Proteomics data following trypsin-digestion as well as pepsin-digestion (Table 1) results in VP1 sequence coverage of 95 and 90 % with the N-terminal coverage starting from residue 25 and 27 indicating additional subpopulations, which are low abundant. Notably, the C-terminus is complete up to several arginine residues (C-Terminal three to six residues), which exclude coverage for both proteins due to small peptides. This suggests exclusive N-Terminal truncation. An assembly into a 60-mer of the full-length VP1 would result in a theoretical *T*=1 mass of 3.54 MDa, VP1 lacking 45 aa would form 3.28 MDa *T*=1 particles. The assigned mass of 3.27 MDa using QToF MS and 3.35 MDa using native CDMS (supplement table S1, note, masses in CDMS are always higher indicating incomplete desolvation) suggests that detected 60-mer particles are indeed formed mainly from VP1 lacking at least 45 aa. To conclude, in this case, heterologous expression of GII.4 Saga VP1 results in a truncated VP1 species with the mere ability to form *T*=1 but not *T*=3 particles.

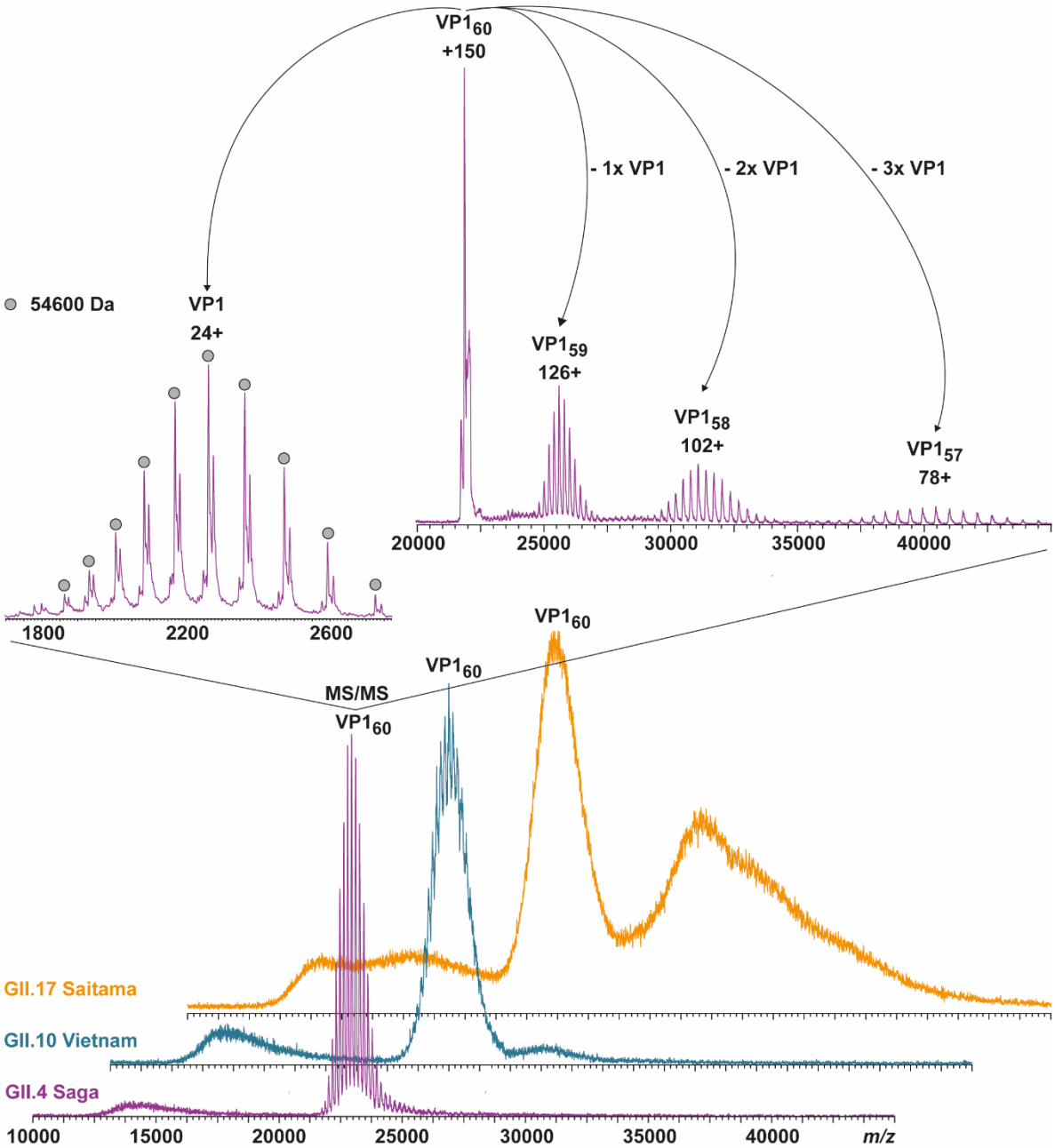

Figure 1. Native MS of different hNoVLPs suggests that a major truncation of VP1 leads to *T*=1 particles. From bottom to top spectra of GII.4 Saga (purple), GII.10 Vietnam (blue) and GII.17 Saitama (orange) in 250 mM ammonium acetate pH 7 at 10 µM VP1 are shown. All variants have main ion distributions between 20,000 and 25,000 *m/z*, which are assigned to $VP1_{60}$ complexes. Collision-induced dissociation MS/MS is shown exemplarily for GII.4 Saga. The dissociation of the 150+ charged $VP1_{60}$ into VP1-monomer (top left) and residual VP1 59-, 58-, and 57-mer (top right) is shown. Charge states and average monomer mass are annotated. The MS/MS confirms stoichiometry assignment and reveals monomer truncation. GII.10 Vietnam and especially GII.17 Saitama also form larger assemblies as indicated by additional signal above 25,000 *m/z*.

242 *3.2 T=1 capsid formation is genotype-independent*

243 Additional hNoVLPs are investigated to pinpoint whether the truncation seen in GII.4 Saga
244 causes *T*=1 formation. Norovirus particle polymorphism has been described as putatively genotype-
245 dependent. Therefore, we extend our sampling to GII.10 Vietnam and GII.17 Saitama (Figure 1). In
246 line with GII.4 Saga measurements, most abundant peak distributions are assigned to VP1 60-mers
247 for both variants. Notably, more acceleration energy compared to GII.4 Saga is needed to gain
248 charge-resolution for VP1 60-mer peaks, which indicates increased VP1 heterogeneity in these
249 samples (Supplement Figure S1). Furthermore, *T*=1 ions in GII.10 Vietnam show tailing with a non-
250 resolved shoulder peak, indicating either aggregation or a further low-intensity assembly of slightly
251 higher mass. In GII.17 Saitama mass spectra, heterogeneity is even more prominent as multiple
252 higher-mass assemblies give rise to complex ion distributions between 30,000 and 40,000 *m*/*z*. GII.17
253 Saitama ion distributions are overlapping with the respective *T*=3 *m*/*z* range observed in previous
254 mass spectra but clear mass assignment is hindered due to high heterogeneity in the sample.
255 Dissociated VP1 monomer species for all listed variants except GII.17 Saitama, where signal
256 intensities are too low for selective dissociation experiments and monomer mass is inferred from
257 CDMS (table S1), are listed in Table 1. If a similar incomplete desolvation for GII.17 Saitama as for
258 GII.4 Saga is assumed in CDMS, the VP1 monomer mass further reduces by ~1500 Da
259 corresponding to additional 14 aa missing resulting in a total of 9 aa closer to the values observed
260 for the other hNoVLPs. Mutual in most VP1 monomer measurements is a major truncation of at
261 least 45 aa (45 aa in GII.4, 45 aa in GII.10, and 20 aa/31 aa in GII.17). Although VP1 truncation is
262 similar in all three variants, the putative cleavage site does not reside in a conserved region and a
263 putative protease cannot be assigned (Table 1).

264 **Table 1.** Overview of investigated samples forming mainly *T*=1 particles. Theoretical (th.) VP1 mass
265 and aa number given for constructs West Chester, Saga, Vietnam and Saitama constructs.
266 Experimental (exp) mass and truncation given for main observed monomeric species after
267 dissociation in conventional MS for all variants except GII.17 Saitama. For Saitama, mass was
268 approximated using CDMS (Table S1). MW molecular weight

Variant	**VP1 th.**	**VP1 exp.**	**Putative cleavage site**	**Trypsin digestion**	**Pepsin digestion**
	MW, total	**Main species MW truncation**	**According to exp. VP1 MW**	**Sequence coverage %, minimal N-terminal truncation**	
GI.1 West Chester	56609 Da, 530 aa	52760 Da, – 40 aa	LAMDPVAGSS/ TAVATAGQVN	80 %, -6 aa	98 %, -3 aa
GII.4 Saga	59005 Da 540 aa	54600 Da, -45 aa	AIAAPVAGQQ/ NVIDPWIRNN	95 %, -25 aa	90 %, -27 aa
GII.10 Vietnam	59901 Da 548 aa	55560 Da, -45 aa	SLAAPVTGQT/ NIIDPWIRMN	94 %, -27 aa	94 %, -27 aa
GII.17 Saitama	58957 Da 540 aa	57300 Da, -17 aa	SNDGATGLVP/ EINNETLPLE	91 %, -32 aa	99 %, -3 aa

269
270

3.3 Heterologous expression of GI.1 West Chester results in either T=1 or T=3 preparations

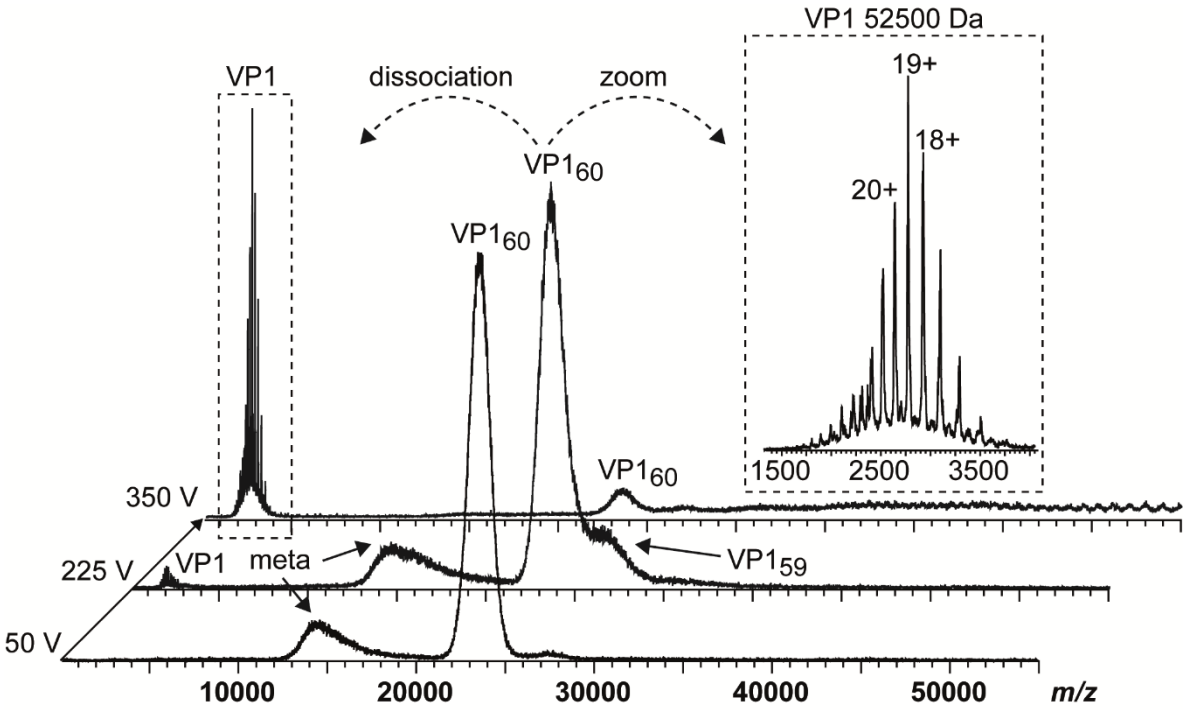

Figure 2. Native MS of a GI.1 West Chester batch forming merely VP1$_{60}$ complexes. Dissociation pathway without selection in the quadrupole is shown for GI.1 West Chester in 250 mM ammonium acetate pH 7 at 10 μM VP1. From bottom to top, illustrative mass spectra are shown for 50 V, 225 V and 350 V acceleration into the collision cell. While at 225 V VP1 monomers dissociate with the main population of VP1 60-mer still intact, signal ratio of VP1 monomer:60-mer are reversed at 350 V. An insert shows a zoom of dissociated VP1 monomer with annotated charge states and average mass. As lower mass ions at approximately 15,000 *m/z* are annotated as metastable ions (meta), monomer lacking at least 43 aa most likely dissociate from *T*=1 species.

To provide further evidence of truncation influence, we compare two GI.1 West Chester batches. Batch 1 is identical to the sample used in our previous work (25). In the second batch, no *T*=3 particles are detected at neutral pH using native MS (Figure 2). The main peak distribution is assigned to *T*=1 particles, which is accompanied by a low-intense shoulder peak comparable to GII.10 Vietnam. At increased acceleration voltage, the *T*=1 ions release VP1 monomers. A close-up of these monomers shows that there are at least two subspecies present. This directly contributes to heterogeneity and therefore low peak resolution of higher-mass species. The dominating VP1 species is assigned to 52760 ± 10 Da, or the theoretical VP1 mass lacking 40 N-terminal aa. Proteomics data, which hint to subspecies with minor truncations, is consistent with other variants tested in this study (Table 1). In our previous study, we could identify GI.1 West Chester VP1 monomers with the major species lacking only three amino acids forming mainly *T*=3 particles (25). Taken together, we can assume that with the VP1 N-terminus of GI.1 West Chester lacking three amino acids the formation of *T*=3 particles is possible, while with an expanded truncation of 43 amino acids this is no longer the case.

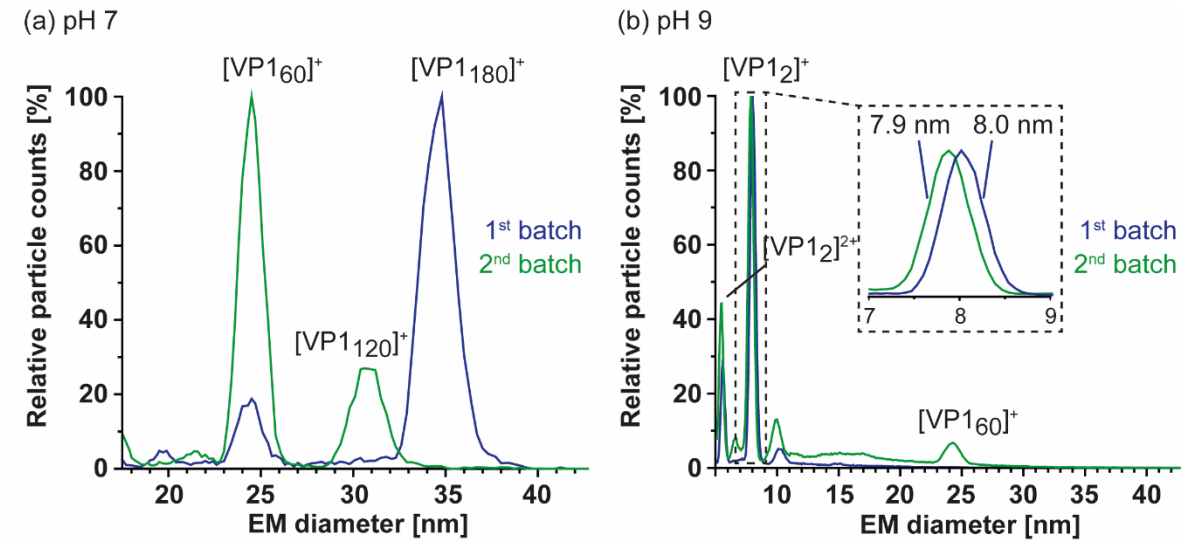

Figure 3. Comparison of two GI.1 West Chester VLP preparations using nES GEMMA. Illustrative spectra are shown for both samples in 40 mM ammonium acetate at pH 7 (a) and pH 9 (b) at approximately 2-10 µM VP1. Depicted are exemplary spectra for two batches in blue (1) and green (2). (a) Batch 1 shows a clear pattern with a main population of 34.37 ± 0.13 nm and less particle counts at 24.09 ± 0.27 nm, assigned to VP1 180-mer and VP1 60mer. In batch 2, VP1 60-mer detected at 24.50 ± 0.12 nm is the most abundant species. Furthermore, a species at 30.71 ± 0.17 nm assigned to VP1 120-mer is present and VP1 180-mer is missing. (b) At pH 9, no VP1 complexes other than VP1 dimer were detected for batch 1. The second batch shows a small particle distribution at 24.18 ± 0.06 indicating higher stability of VP1 60-mers. A zoom at the low EMD range depicts a minor difference in VP1 dimer size of 8.03 ± 0.01 nm for batch 1 and 7.89 ± 0.01 nm for batch 2. For both conditions, shown EMD range was adjusted and the complete range including multiply charged species in the low EMD range are shown in supplement Figure S2.

Furthermore, we characterize particle size and stoichiometry in further detail using nES GEMMA. Measurements of both GI.1 West Chester preparations are superimposed in Figure 3. In order to exclude artefacts, all samples are measured at different dilutions (supplement Figure S2). Putative artefacts include unspecific, nES based aggregates at high sample concentration, as well as multiply charged particles obtained at low percentage values during charge equilibration in the bipolar atmosphere of the spray chamber. Comparison of both batches at neutral pH reveals a clear shift in particle size and their counts. In the first GI.1 West Chester batch most prominent particle counts are at 34.37 ± 0.13 nm, which are assigned to *T*=3 particles. Further particle counts at 8.01 ± 0.01 nm and 24.09 ± 0.17 nm are assigned to VP1 dimer and VP1 60-mer. nES GEMMA spectra of the second batch show a predominant species at 24.50 ± 0.12 nm equaling *T*=1, as well as a species with low counts at 30.71 ± 0.17 nm. The population at 30.71 nm was assigned to 6.24 MDa using VLP correlation fitting approximately 120 VP1 (28). At pH9, high-mass particles in batch 1 are fragile, complementing our previous findings with native MS (25), while the *T*=1 VLPs in batch 2 are resistant to pH 9. Other particles in the second batch bigger than 24.18 ± 0.06 nm disappear. Interestingly, comparing EMDs of this 60-mer species at neutral pH and pH 9 does not indicate swelling or shrinking of the particles. Notably, the VP1 dimers released in alkaline conditions are slightly smaller in the second batch in line with the observed truncation. Moreover, size difference is not observed for *T*=1 particles in the two batches in line with an N-terminal truncation located at the inner face of the capsids. We can conclude that no *T*=3 particles are detected with nES GEMMA in the second West Chester batch, which indicates that at least a certain amount of full-length or less truncated VP1 subpopulation is needed to form *T*=3 particles. Intermediate-sized populations could stem from either truncated, full-length VP1 or a mixture.

3.4 Detailed nES GEMMA and CDMS profiling

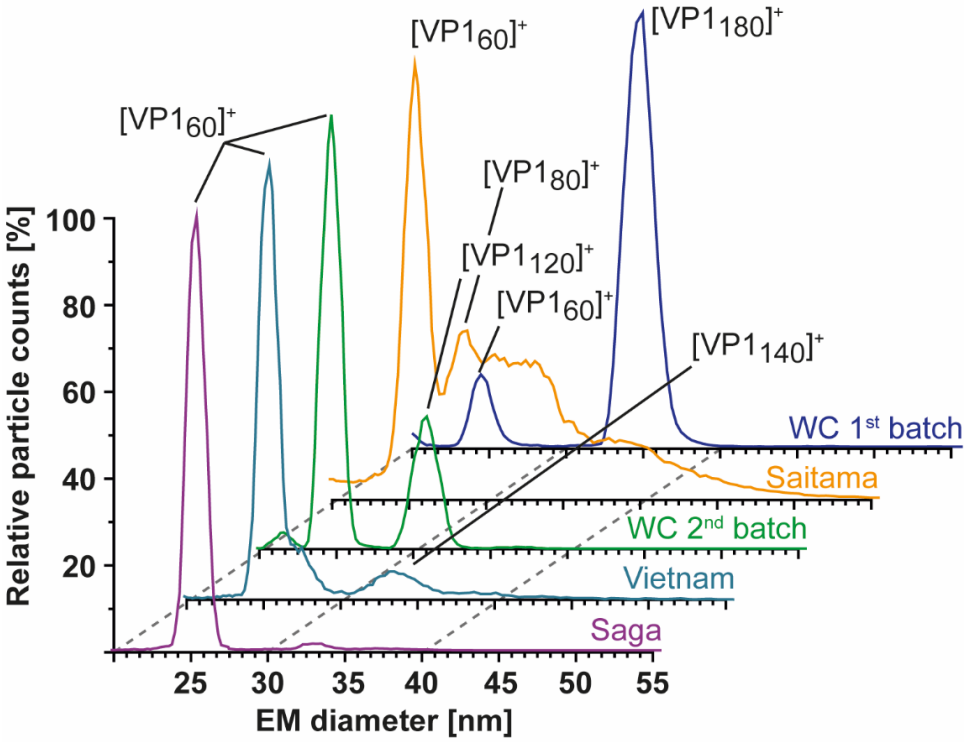

Figure 4. Size-distribution overview of different hNoVLPs with nES GEMMA. All variants are measured at 40 mM ammonium acetate pH 7 and approximately 2-10 µM VP1. From bottom to top GII.4 Saga (purple), GII.10 Vietnam (light blue), West Chester batch 2 (WC, green), GII.17 Saitama (orange) and West Chester batch 1 (WC, dark blue). West Chester batch 1 is shown as an indication of the expected EMD range for *T*=3 particles. Assigned species are annotated. VP1 60-mers were detected in all variants, with less counts in WC batch 1. Next to 60-mers, GII.4 Saga and GII.10 Vietnam show distributions at approx. 33 nm assigned to VP1 140-mer and WC second batch shows a distinct peak at 30 nm assigned to VP1-120mer. In GII.17 Saitama, at least two peaks can be fitted in the particle distribution accompanying VP1 60-mer annotated as VP1 80-mer and putatively VP1 180-mer.

As nES GEMMA is fast and sensitive all samples are further profiled to see if *T*=3 assemblies can be rescued and/or *T*=1 particles from truncated VP1 are in general more stable at alkaline pH. At neutral pH and low ionic strength, particle size patterns of all variants are in line with conventional native MS. Next to GI.1 Wester Chester second batch, GII.4 Saga and GII. 10 Vietnam form *T*=1 particles but not *T*=3 particles. GII.17 Saitama shows some signals, which may originate from *T*=3 particles. Similar to the low-count species in GI.1 West Chester batch 2 of 32.62± 0.22 nm (120-mer), in GII.4 Saga and even more prominent in GII.10 Vietnam further particles are detected at around 33 nm equaling 7.7 MDa (VP1 140-mer). In line with native MS data, enormous heterogeneity is observed in GII.17 Saitama, multiple other species than VP1 60-mer can be distinguished with nES GEMMA (Figure 4). Measurements at pH 5 up to pH 9 reveal that *T*=1 formations of all samples are mostly resistant to changing solution conditions (Figure 5). Starting from pH 8, free VP1 dimer was detected in all variants in low counts. At pH 9, GII.10 Vietnam and GII.17 Saitama show reversed particle count ratios of VP1 60-mer and VP1 dimer. Interestingly, also the larger assemblies are still observable. In GII.4 Saga, no complexes are detected at pH 9 and the employed low VP1 concentrations. However, GII.4 Saga 60-mers remain intact at alkaline pH and low ionic strength in conventional native MS measurements at 10 µM VP1 (50 mM ammonium acetate, supplement Figure S3). For all samples, particle-size patterns are also consistent at pH 5, although with lower particle counts and with increased background noise. Taken together, this indicates that *T*=1 particles are highly stable resisting alkaline pH and *T*=3 particle formation cannot be rescued by changing solution conditions.

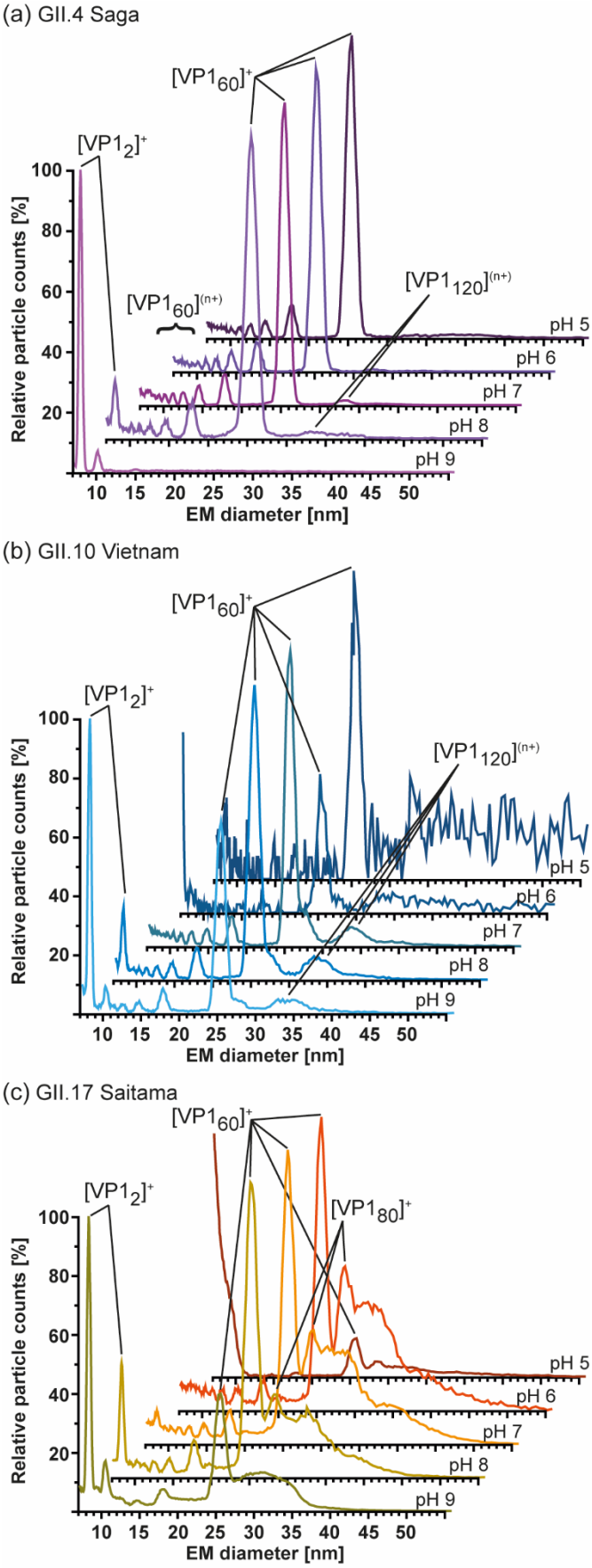

Figure 5. Measurements at different pH of hNoVLPs with GEMMA indicates high pH-resistance of *T*=1 particles formed from truncated VP1. All measurements were performed at 40 mM ammonium acetate at pH 5-9 from top to bottom at approximately 2-10 µM. (a) GII.4 Saga (purple) shows mainly VP1 60-mer accompanied by multiply charged VP1-60-mer. Particle patterns differ only at pH 8, where VP1 dimers are present in low counts as well as pH 9, where merely VP1 dimer is detected. (b) GII.10 Vietnam (blue) show intact *T*=1 particles at all tested pH values. Increased particle counts at pH 7-9 are accompanied with multiply charged VP1 60-mer. Disassembly into VP1 dimer is seen at pH 8 but is only resulting in less $VP1_{60}$ counts at pH 9. This pattern is comparable to measurements of GII.17 Saitama (c). Here, main $VP1_{60}$ species are accompanied by heterogeneous subspecies, which are reduced under alkaline conditions.

So far, several different size-populations are detected outside the scope of Caspar-Klug capsid assembly theory (39), where multiples of 60 (with 120 being formally not allowed) form particles of icosahedral symmetry. CDMS measurements in conditions comparable to our conventional QToF measurements at 250 mM ammonium acetate are used to unambiguously assign such assemblies. For GII.4 Saga, no species but *T*=1 particles are observed in sufficient counts to fit peaks. Albeit peaks at approximately 33 nm appear in low-salt nES GEMMA measurements, no respective peak can be assigned to VP1 140-mer with CDMS. At notably lower ion counts, GII.10 Vietnam shows *T*=1 particles as well as two further species with approximately 4.5 MDa and 6.9 MDa assigned to VP1 79-mer and VP1 121-mer, respectively. Note that those species are approximations due to very low counts and stoichiometry is based on assuming that 60 VP1 form the 3.41 MDa population. For both variants, the VP1

mass inferred from the 60-mer is higher than determined in conventional native MS (CDMS/nMS: GII.4 Saga 55.8/54.6 kDa and GII.10 Vietnam 56.8/55.2 kDa). This indicates mixed subpopulations of different VP1-size forming particles or less efficient desolvation in CDMS compared to QToF measurements. Notably, species at 4.5 MDa and 6.8 MDa are repetitive in GII.10 Vietnam as well as the GI.1 West Chester batch 1 (supplement Figure S4). In GII.17 Saitama, CDMS helps to elucidate mass heterogeneity observed in the other methods. Next to a distinct population of 3.44 MDa assigned to VP1 60-mer, five additional high mass species can be deconvoluted. CDMS clearly shows the absence of fully-formed *T*=3 particles. Proteomics data for Saitama indicates a subpopulation of VP1 with a minor truncation of 3 aa. This subpopulation is putatively able to form *T*=3 particles in low amounts, which are likely prone to disassemble at varying concentration, ionic strength, and pH. Given a mass of approximately 57.3 kDa, CDMS Saitama high-mass species fit VP1 71-, 91-, 100-, 108-, and 120-mers. In contrast, the stability at alkaline pH and low concentrations of these species suggests distinct assemblies. Moreover, although formally not allowed according to Triangulation theory, detected VP1 intermediates are repeatedly found in all tested variants and with different techniques.

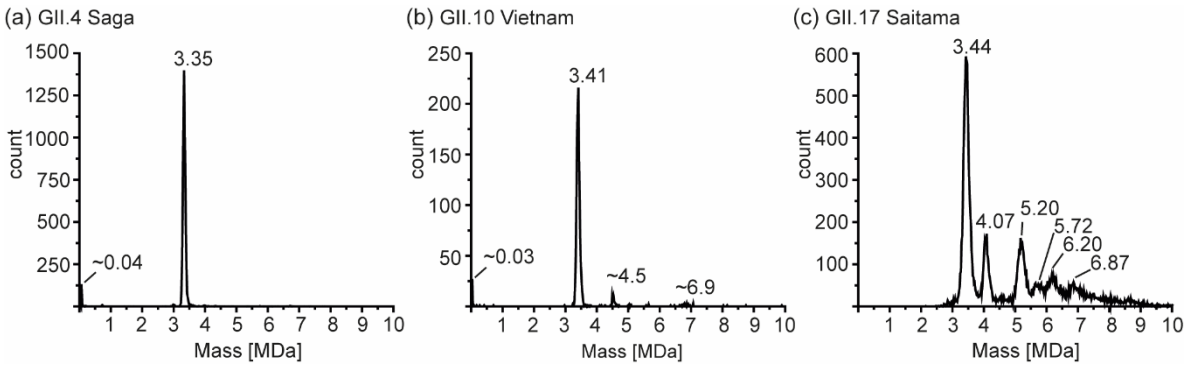

Figure 6. Charge detection mass spectrometry of hNoVLPs at 250 mM ammonium acetate pH 7 and 10 μM VP1. Illustrative spectra shown for (a) GII.4 Saga (b) GII.10 Vietnam and (c) GII.17 Saitama. Distinct peaks are annotated, for GII.4 Saga and GII.10 Vietnam low-count species, masses are approximations.

4. Discussion

In this study, different hNoVLP variants are investigated with a set of biophysical tools in order to obtain insights into particle size, stoichiometry and shape. hNoVLP preparations forming merely *T*=1 particles are identified. *T*=1 particles have repeatedly been described in hNoVLP preparations (19, 21, 24, 25). In our previous study, *T*=1 and *T*=3 particles were coexisting in GI.1 West Chester and GII.17 Kawasaki preparations at neutral pH. In line with a former study on GI.1 Norwalk (24), GI.1 West Chester formed *T*=3 particles, which were prone to disassemble in alkaline pH (25). Here, we identify a major VP1 N-terminal truncation of more than 40 aa in several hNoV variants leading to *T*=1 particles only. The origin of this truncation is unclear. As no clear conserved cleavage motif could be identified, various or unspecific proteases are proposed, likely originating from the insect cell expression system (40, 41). Moreover, this points at a structurally defined proteolytic site, which is in line with the flexibility observed in the N-terminal arm. Notably, in all investigated preparations, less populated subspecies with limited truncations building the observed particle formations cannot be excluded as proteomics data suggests. This is further supported by a *T*=1 structure from cryo-EM (21), which shows no electron density for the N-terminal stretch indicating that it is either flexible or absent in the preparation.

The ability of truncated VP1 to form mainly *T*=1 particles is genogroup- and genotype-independent as several hNoV variants have been targeted here. This indicates a major truncation is sufficient for VP1 to form *T*=1 only and therefore, homogenous, small-sized hNoVLP production is reproducible. Interestingly, several intermediate species have been observed repeatedly. In GI.1 West Chester batch 2, GII.4 Saga, and GII.10 Vietnam intermediates are detected in very low

proportions. In GII.17 Saitama, spectra suggest a heterogeneous size distribution of several high-mass species with increased counts. A repetitive species that overlaps between preparations is VP1 120-mer. VP1 dimer has been described as building block for capsid assembly that suggests that intermediate species must be even integers (14, 15, 42, 43). Therefore, GII.17 Saitama CDMS measurements resulting in odd numbered complexes are rounded here. Using a combination of characterizing tools like nES GEMMA, conventional MS, and CDMS, VP1 120-mer appears biologically relevant although not allowed according to Triangulation theory (39). Moreover, the agreement in GEMMA mass assignment based on a VLP calibration and CDMS reveals that these assemblies resemble hollow spheres like regular capsids. Putative, non-allowed *T*=2 particles have been described for bluetongue virus and brome mosaic virus among others (44-46). Another intermediate observed in different hNoVLP preparations is VP1 80-mer. Interestingly, it is detected in preparations, in which also *T*=3 particles were observed like GI.1 Norwalk (24), GI.1 West Chester (25) (supplement Figure S4). This indicates different behavior of full-length and truncated VP1 and mixtures thereof. General observed particle plasticity suggests that these species could be trapped formations or overgrown-particles as observed for hepatitis B virus and woodchuck hepatitis virus (47, 48). However, it has to be noted that assemblies have specific sizes as evident from CDMS rather than covering a broad distribution. The inability to form full *T*=3 particles indicates that the N-terminus is required to form flat C/C dimers leading to lattice expansion. We already proposed an influence of the N-terminus in capsid size determination in our previous study (25). In turn, the truncated VP1 would likely form mainly bent A/B-like dimers forming the pentameric vertices present in both VLP formations. This would then likely preclude *T*=2 capsids. An alternative assembly route would follow octaedric symmetry, which has been described for SV40 polyomavirus (49). These require strongly bent dimer interactions and a 24-mer octaeder formed from pentamers would exactly match the VP1 120-mers detected here. This interpretation is further appealing as it offers an explanation for the aberrant GII.17 Saitama assemblies of 70/72, 90/92, 100 and 108/110 VP1 subunits being octaeders lacking multiple pentamers. Polymorphism in hNoVLP production, independent of the expression system, has been described both for VP1 forming *T*=1 and *T*=3 particles at neutral pH and intermediates upon changing conditions. In an assembly study on GI.1 Norwalk, three N-terminal deletion mutants were compared (18). Full-length as well as deletion of N-terminal 20 aa resulted still in *T*=3 particles. Deletion of 34 and 98 aa N-terminally did not result in any particles detectable with electron microscopy. However, N-terminal 34 aa mutant expression was described as low, hampering the assessment of how this deletion is involved in capsid assembly. Furthermore, N-terminal deletions of 26 aa and 38 aa were introduced in GII.4 Sydney VLPs. Both constructs were found to form mainly small particles when examined with electron microscopy (50). Next to deletion itself, culture conditions were also described as a putative reason for size heterogeneity. Another attempt to gain size-homogeneity in hNoVLP preparations was performed by Someya et al using GI.4 Chiba VLPs (51). Truncation of 45 aa N-terminally, similar as observed in this study, was identified and the subsequent introduction of a mutation Leu43Val in this region resulted in the formation of merely *T*=3 particles. However, in a follow-up study, GI.4 Chiba mutants were shown to form 23 nm or *T*=1 particles, putatively due to freezing and thawing of preparations or pH-dependent processes (52). Previously, *T*=4 particles were identified in hNoVLP preparations (20, 21). Interestingly, one study included GII.2 Snow Mountain virus forming *T*=1 particles (21). Here, residues 1 to 46 were not covered in electron density maps. Hence, truncation as origin of small particles similar to our observations cannot be excluded.

Next to particle size distribution, the influence of solution pH was investigated. *T*=1 particles, as well as higher-mass assemblies in GII.17 Saitama, were found to be pH-independent. Moreover, in preparations forming mainly *T*=1 particles, like GI.1 West Chester batch 2, *T*=1 particles showed increased stability in alkaline conditions. Therefore, truncated VP1 is able to build particles with increased stability. This implies great advances for bionanotechnology as especially in approaches using VLPs as carrier particles need to be stable independently of environmental conditions. The

contribution of the N-terminus to pH stability suggests a way to obtain S-particles of increased stability by truncation.

There is no hNoV vaccine available yet and hNoVLP size polymorphism could contribute to this circumstance. Therefore, N-terminally truncated particles have great potential to be beneficial as they imply size homogeneity. Furthermore, these particles have intact protrusions, which are necessary for antigen recognition and putatively enable other immunological approaches like antigen presentation. However, whether the altered orientation, and therefore interaction between dimeric protrusions affects antibody raising, needs to be investigated. Additionally, increased stability would likely allow simplified and prolonged storage. Our results indicate that such small particles from truncated VP1 can be produced independent of genotype by introducing N-terminal deletion mutants.

Author Contributions: Conceptualization, CU; methodology, CU, MFJ, GA.; validation, RP; formal analysis, RP, VW; investigation, RP, VW, SZ, KB, NL, JD, CK.; resources, CU, MFJ, GA.; data curation, RP.; writing—original draft preparation, RP, CU.; writing—review and editing, all.; visualization, RP.; supervision, CU.; project administration, CU.; funding acquisition, CU. All authors have read and agreed to the published version of the manuscript.

Funding: The Heinrich-Pette-Institute, Leibniz Institute for Experimental Virology is supported by the Free and Hanseatic City Hamburg and the federal ministry of health (Bundesministerium für Gesundheit, BMG). CU acknowledges funding from the Leibniz Association through SAW-2014-HPI-4 grant. RP, JMG, CU and CMF acknowledge funding from EU Horizon 2020 project VIRUSCAN 731868. RP further acknowledges funding from MIN Graduate School Universität Hamburg. JD was funded by DFG FOR2327 Virocarb. VUW acknowledges funding of the Austrian Theodor Körner Fonds. VUW and RP both acknowledge funding of COST Action BM1403 Native Mass Spectrometry and Related Methods for Structural Biology.

Acknowledgments: We thank Grant Hansman for providing VLPs.

Conflicts of Interest: The authors declare no conflict of interest.

536 **References**

537 1. Ahmed SM, Hall AJ, Robinson AE, Verhoef L, Premkumar P, Parashar UD, et al. Global prevalence of
538 norovirus in cases of gastroenteritis: a systematic review and meta-analysis. Lancet Infect Dis. 2014;14(8):725-
539 30.
540 2. Teunis PF, Moe CL, Liu P, Miller SE, Lindesmith L, Baric RS, et al. Norwalk virus: how infectious is it?
541 J Med Virol. 2008;80(8):1468-76.
542 3. Xi JN, Graham DY, Wang KN, Estes MK. Norwalk virus genome cloning and characterization.
543 Science. 1990;250(4987):1580-3.
544 4. Jiang X, Wang M, Wang K, Estes MK. Sequence and genomic organization of Norwalk virus.
545 Virology. 1993;195(1):51-61.
546 5. Chhabra P, de Graaf M, Parra GI, Chan MC, Green K, Martella V, et al. Updated classification of
547 norovirus genogroups and genotypes. J Gen Virol. 2019;100(10):1393-406.
548 6. Kapikian AZ, Wyatt RG, Dolin R, Thornhill TS, Kalica AR, Chanock RM. Visualization by immune
549 electron microscopy of a 27-nm particle associated with acute infectious nonbacterial gastroenteritis. J Virol.
550 1972;10(5):1075-81.
551 7. Eden JS, Tanaka MM, Boni MF, Rawlinson WD, White PA. Recombination within the Pandemic
552 Norovirus GII.4 Lineage. Journal of Virology. 2013;87(11):6270-82.
553 8. de Graaf M, van Beek J, Vennema H, Podkolzin AT, Hewitt J, Bucardo F, et al. Emergence of a novel
554 GII.17 norovirus - End of the GII.4 era? Eurosurveillance. 2015;20(26):8-15.
555 9. Ettayebi K, Crawford SE, Murakami K, Broughman JR, Karandikar U, Tenge VR, et al. Replication of
556 human noroviruses in stem cell-derived human enteroids. Science. 2016.
557 10. Tome-Amat J, Fleischer L, Parker SA, Bardliving CL, Batt CA. Secreted production of assembled
558 Norovirus virus-like particles from Pichia pastoris. Microb Cell Fact. 2014;13:134.
559 11. Taube S, Kurth A, Schreier E. Generation of recombinant norovirus-like particles (VLP) in the human
560 endothelial kidney cell line 293T. Arch Virol. 2005;150(7):1425-31.
561 12. Diamos AG, Mason HS. High-level expression and enrichment of norovirus virus-like particles in
562 plants using modified geminiviral vectors. Protein Expr Purif. 2018;151:86-92.
563 13. Mason HS, Ball JM, Shi JJ, Jiang X, Estes MK, Arntzen CJ. Expression of Norwalk virus capsid protein
564 in transgenic tobacco and potato and its oral immunogenicity in mice. Proc Natl Acad Sci U S A.
565 1996;93(11):5335-40.
566 14. Prasad BV, Rothnagel R, Jiang X, Estes MK. Three-dimensional structure of baculovirus-expressed
567 Norwalk virus capsids. J Virol. 1994;68(8):5117-25.
568 15. Prasad BV, Hardy ME, Dokland T, Bella J, Rossmann MG, Estes MK. X-ray crystallographic structure
569 of the Norwalk virus capsid. Science. 1999;286(5438):287-90.
570 16. Jiang X, Wang M, Graham DY, Estes MK. Expression, self-assembly, and antigenicity of the Norwalk
571 virus capsid protein. J Virol. 1992;66(11):6527-32.
572 17. Tan M, Jiang X. The p domain of norovirus capsid protein forms a subviral particle that binds to histo-
573 blood group antigen receptors. J Virol. 2005;79(22):14017-30.
574 18. Bertolotti-Ciarlet A, White LJ, Chen R, Prasad BV, Estes MK. Structural requirements for the assembly
575 of Norwalk virus-like particles. J Virol. 2002;76(8):4044-55.
576 19. White LJ, Hardy ME, Estes MK. Biochemical characterization of a smaller form of recombinant
577 Norwalk virus capsids assembled in insect cells. J Virol. 1997;71(10):8066-72.

578 20. Devant JM, Hofhaus G, Bhella D, Hansman GS. Heterologous expression of human norovirus GII.4
579 VP1 leads to assembly of T=4 virus-like particles. Antiviral Res. 2019;168:175-82.
580 21. Jung J, Grant T, Thomas DR, Diehnelt CW, Grigorieff N, Joshua-Tor L. High-resolution cryo-EM
581 structures of outbreak strain human norovirus shells reveal size variations. Proc Natl Acad Sci U S A.
582 2019;116(26):12828-32.
583 22. Taniguchi K, Urasawa S, Urasawa T. Further studies of 35--40 nm virus-like particles associated with
584 outbreaks of acute gastroenteritis. J Med Microbiol. 1981;14(1):107-18.
585 23. Dulfer J, Kadek A, Kopicki JD, Krichel B, Uetrecht C. Structural mass spectrometry goes viral. Adv
586 Virus Res. 2019;105:189-238.
587 24. Shoemaker GK, van Duijn E, Crawford SE, Uetrecht C, Baclayon M, Roos WH, et al. Norwalk virus
588 assembly and stability monitored by mass spectrometry. Mol Cell Proteomics. 2010;9(8):1742-51.
589 25. Pogan R, Schneider C, Reimer R, Hansman G, Uetrecht C. Norovirus-like VP1 particles exhibit isolate
590 dependent stability profiles. J Phys Condens Matter. 2018;30(6):064006.
591 26. Kaufman SL, Skogen JW, Dorman FD, Zarrin F, Lewis KC. Macromolecule analysis based on
592 electrophoretic mobility in air: globular proteins. Anal Chem. 1996;68(11):1895-904.
593 27. Weiss VU, Bereszcazk JZ, Havlik M, Kallinger P, Gosler I, Kumar M, et al. Analysis of a common cold
594 virus and its subviral particles by gas-phase electrophoretic mobility molecular analysis and native mass
595 spectrometry. Anal Chem. 2015;87(17):8709-17.
596 28. Weiss VU, Pogan R, Zoratto S, Bond KM, Boulanger P, Jarrold MF, et al. Virus-like particle size and
597 molecular weight/mass determination applying gas-phase electrophoresis (native nES GEMMA). Anal Bioanal
598 Chem. 2019;411(23):5951-62.
599 29. Hansman GS, Natori K, Oka T, Ogawa S, Tanaka K, Nagata N, et al. Cross-reactivity among sapovirus
600 recombinant capsid proteins. Arch Virol. 2005;150(1):21-36.
601 30. Hansman GS, Saito H, Shibata C, Ishizuka S, Oseto M, Oka T, et al. Outbreak of gastroenteritis due to
602 sapovirus. J Clin Microbiol. 2007;45(4):1347-9.
603 31. Laemmli UK. Cleavage of structural proteins during the assembly of the head of bacteriophage T4.
604 Nature. 1970;227(5259):680-5.
605 32. Shevchenko A, Tomas H, Havlis J, Olsen JV, Mann M. In-gel digestion for mass spectrometric
606 characterization of proteins and proteomes. Nat Protoc. 2006;1(6):2856-60.
607 33. van den Heuvel RH, van Duijn E, Mazon H, Synowsky SA, Lorenzen K, Versluis C, et al. Improving
608 the performance of a quadrupole time-of-flight instrument for macromolecular mass spectrometry. Anal
609 Chem. 2006;78(21):7473-83.
610 34. Lorenzen K, Versluis C, van Duijn E, van den Heuvel RHH, Heck AJR. Optimizing macromolecular
611 tandem mass spectrometry of large non-covalent complexes using heavy collision gases. International Journal
612 of Mass Spectrometry. 2007;268(2):198-206.
613 35. Morgner N, Robinson CV. Massign: an assignment strategy for maximizing information from the
614 mass spectra of heterogeneous protein assemblies. Anal Chem. 2012;84(6):2939-48.
615 36. Contino NC, Pierson EE, Keifer DZ, Jarrold MF. Charge detection mass spectrometry with resolved
616 charge states. J Am Soc Mass Spectrom. 2013;24(1):101-8.
617 37. Tycova A, Prikryl J, Foret F. Reproducible preparation of nanospray tips for capillary electrophoresis
618 coupled to mass spectrometry using 3D printed grinding device. Electrophoresis. 2016;37(7-8):924-30.

619 38. Bacher G, Szymanski WW, Kaufman SL, Zollner P, Blaas D, Allmaier G. Charge-reduced nano
620 electrospray ionization combined with differential mobility analysis of peptides, proteins, glycoproteins,
621 noncovalent protein complexes and viruses. J Mass Spectrom. 2001;36(9):1038-52.
622 39. Caspar DL, Klug A. Physical principles in the construction of regular viruses. Cold Spring Harb Symp
623 Quant Biol. 1962;27:1-24.
624 40. Gotoh T, Miyazaki Y, Kikuchi K, Bentley WE. Investigation of sequential behavior of carboxyl
625 protease and cysteine protease activities in virus-infected Sf-9 insect cell culture by inhibition assay. Appl
626 Microbiol Biotechnol. 2001;56(5-6):742-9.
627 41. Gotoh T, Ono H, Kikuchi K, Nirasawa S, Takahashi S. Purification and characterization of aspartic
628 protease derived from Sf9 insect cells. Biosci Biotechnol Biochem. 2010;74(10):2154-7.
629 42. Uetrecht C, Barbu IM, Shoemaker GK, van Duijn E, Heck AJ. Interrogating viral capsid assembly with
630 ion mobility-mass spectrometry. Nat Chem. 2011;3(2):126-32.
631 43. Pogan R, Dulfer J, Uetrecht C. Norovirus assembly and stability. Curr Opin Virol. 2018;31:59-65.
632 44. Grimes JM, Burroughs JN, Gouet P, Diprose JM, Malby R, Zientara S, et al. The atomic structure of the
633 bluetongue virus core. Nature. 1998;395(6701):470-8.
634 45. Baker TS, Olson NH, Fuller SD. Adding the third dimension to virus life cycles: three-dimensional
635 reconstruction of icosahedral viruses from cryo-electron micrographs. Microbiol Mol Biol Rev. 1999;63(4):862-
636 922, table of contents.
637 46. Krol MA, Olson NH, Tate J, Johnson JE, Baker TS, Ahlquist P. RNA-controlled polymorphism in the
638 in vivo assembly of 180-subunit and 120-subunit virions from a single capsid protein. Proc Natl Acad Sci U S
639 A. 1999;96(24):13650-5.
640 47. Lutomski CA, Lyktey NA, Zhao Z, Pierson EE, Zlotnick A, Jarrold MF. Hepatitis B Virus Capsid
641 Completion Occurs through Error Correction. J Am Chem Soc. 2017;139(46):16932-8.
642 48. Pierson EE, Keifer DZ, Kukreja AA, Wang JC, Zlotnick A, Jarrold MF. Charge Detection Mass
643 Spectrometry Identifies Preferred Non-Icosahedral Polymorphs in the Self-Assembly of Woodchuck Hepatitis
644 Virus Capsids. J Mol Biol. 2016;428(2 Pt A):292-300.
645 49. Salunke DM, Caspar DL, Garcea RL. Polymorphism in the assembly of polyomavirus capsid protein
646 VP1. Biophys J. 1989;56(5):887-900.
647 50. Huo YQ, Wan X, Wang ZJ, Meng SL, Shen S. Production of Norovirus VLPs to size homogeneity.
648 Virus Research. 2015;204:1-5.
649 51. Someya Y, Shirato H, Hasegawa K, Kumasaka T, Takeda N. Assembly of homogeneous norovirus-like
650 particles accomplished by amino acid substitution. J Gen Virol. 2011;92(Pt 10):2320-3.
651 52. Hasegawa K, Someya Y, Shigematsu H, Kimura-Someya T, Nuemket N, Kumasaka T. Crystallization
652 and X-ray analysis of 23 nm virus-like particles from Norovirus Chiba strain. Acta Crystallogr F Struct Biol
653 Commun. 2017;73(Pt 10):568-73.
654

655